ADOLESCENT DEVELOPMENT OF MULTISCALE CORTICAL WIRING AND FUNCTIONAL CONNECTIVITY IN THE HUMAN CONNECTOME

Bo-yong Park[1,2,3*], Casey Paquola[1,4], Richard A. I. Bethlehem[5,6], Oualid Benkarim[1], Neuroscience in Psychiatry Network (NSPN) Consortium[†], Bratislav Mišić[1], Jonathan Smallwood[7], Edward T. Bullmore[6], Boris C. Bernhardt[1*]

[1]McConnell Brain Imaging Centre, Montreal Neurological Institute and Hospital, McGill University, Montreal, Quebec, Canada; [2]Department of Data Science, Inha University, Incheon, Republic of Korea; [3]Center for Neuroscience Imaging Research, Institute for Basic Science, Suwon, Republic of Korea; [4]Institute of Neuroscience and Medicine (INM-1), Forschungszentrum Jülich, Jülich, Germany; [5]Autism Research Centre, Department of Psychiatry, University of Cambridge, Cambridge, United Kingdom; [6]Brain Mapping Unit, Department of Psychiatry, University of Cambridge, Cambridge, United Kingdom; [7]Queen's University, Kingston, ON, Canada

[†]A complete list of investigators from the Neuroscience in Psychiatry Network (NSPN) Consortium can be found in the Supporting Information.

*** Corresponding Authors:**

Bo-yong Park, PhD
Department of Data Science
Inha University
Incheon, Republic of Korea
Phone: +82-32-860-9427
Email: boyong.park@inha.ac.kr

Boris C. Bernhardt, PhD
Multimodal Imaging and Connectome Analysis Lab
McConnell Brain Imaging Centre
Montreal Neurological Institute and Hospital
McGill University
Montreal, Quebec, Canada
Phone: +1-514-398-3579
Email: boris.bernhardt@mcgill.ca

ABSTRACT

Adolescence is a time of profound changes in the structural wiring of the brain and maturation of large-scale functional interactions. Here, we analyzed structural and functional brain network development in an accelerated longitudinal cohort spanning 14–25 years (n = 199). Core to our work was an advanced model of cortical wiring that incorporates multimodal MRI features of (i) cortico-cortical proximity, (ii) microstructural similarity, and (iii) diffusion tractography. Longitudinal analyses assessing age-related changes in cortical wiring during adolescence identified increases in cortical wiring within attention and default-mode networks, as well as between transmodal and attention, and sensory and limbic networks, indicative of a continued differentiation of cortico-cortical structural networks. Cortical wiring changes were statistically independent from age-related cortical thinning seen in the same subjects. Conversely, resting-state functional MRI analysis in the same subjects indicated an increasing segregation of sensory and transmodal systems during adolescence, with age-related reductions in their functional connectivity alongside with an increase in structural wiring distance. Our findings provide new insights into adolescent brain network development, illustrating how the maturation of structural wiring interacts with the development of macroscale network function.

KEYWORDS: adolescence; multiscale cortical wiring; functional network communication

INTRODUCTION

Adolescence is characterized by ongoing cognitive and biological development, and increasing evidence suggests that co-maturation of structural and functional brain networks during that time window underpin broad cognitive development [1–9]. With advances in neuroimaging techniques, particularly magnetic resonance imaging (MRI) acquisition and modelling, it has become possible to chart microstructural and macroscale brain organization *in vivo*. Prior MRI literature has assessed regional changes in brain structure [1–3,10–16], showing age-related widespread decreases in cortical thickness [1,13], as well as increases in intracortical myelin [15–17]. Complementing these regional changes, diffusion and functional MRI studies showed an ongoing maturation of both the microstructure of inter-connecting white matter tracts as well as large-scale developmental changes in functional network organization, indicative of shifts in brain connectivity towards a more distributed topology [18–20]. Utilizing multimodal longitudinal MRI analyses, here, we explored how adolescent structural network development gives rise to potential shifts in functional network architecture.

Core to our work is a comprehensive and recently introduced model of cortical wiring, which integrates several *in vivo* features of structural connectivity *i.e.*, diffusion MRI tractography, geodesic distance mapping, and microstructural covariance analysis [21]. Diffusion MRI tractography maps white matter fibers, showing increasing validity in approximating deeper tracts, but some limitations in the proximity of cortical grey matter regions [22,23]. On the other hand, geodesic distance analysis measures the spatial proximity of areas across the cortical sheet, tapping into short range cortico-cortical connectivity and wiring cost [24]. Finally, a recent extension of structural covariance analysis [25,26], labelled microstructural profile covariance analysis, identifies networks with similar myelin-sensitive imaging characteristics across cortical depths in a subject-specific manner [27,28]. By integrating the complementary connectivity measures from diffusion MRI tractography, geodesic distance, and microstructural covariance via unsupervised machine learning, we can generate a multiscale cortical coordinate system, and arrange cortical regions with respect to their similarity in structural wiring [21]. In a prior evaluation in healthy adults, we demonstrated that this approach captures spatial gradients of (i) cortical cytoarchitecture, (ii) cell-type specific gene expression, and (iii) intrinsic functional connectivity and signal flow measured from resting-state functional MRI and intracranial electrical recordings [21], supporting neurobiological and functional validity. Here, we adopted this wiring model to chart adolescent development of structural brain networks longitudinally.

As brain structure ultimately scaffolds brain function [29–35], it is not surprising that multiple functional networks also change in parallel throughout adolescence. Prior analyses based on resting-state functional MRI connectivity analysis in youth have shown shifts in connectivity patterns in higher order cortical networks, particularly the default mode and frontoparietal networks, both known to be spatially distributed [3,36,37]. In one recent study, it was furthermore shown that different cortical areas undergo variable trajectories of functional maturation, differentiating sensory and motor systems that follow a more 'conservative' functional trajectory from transmodal systems that show a more 'disruptive' mode, reflected by reconfiguration of their functional connectivity patterns towards a more distributed, long-range connectional architecture [37]. Benefitting from an increasing availability of multimodal datasets, several studies have begun to examine how brain structure and function co-mature. For example, a prior study showed that structural network modules become more segregated with advancing age, and that this process reflects ongoing development of executive function from 8 to 22 years [38]. In a follow-up study, the authors showed increases in structure-function coupling, particularly in transmodal cortices [3]. Another recent study showed consistent findings that the correspondence of structural and functional networks is preserved in transmodal regions across the adult lifespan, while sensorimotor systems showed a decreasing trend of structure-function coupling [39]. In the current work, we built on this growing literature to assess how adolescent changes in multiscale cortical wiring are associated with changes in brain network function.

Our study was based on the Neuroscience in Psychiatry Network (NSPN) 2400 cohort, an accelerated longitudinal dataset that enrolled healthy individuals between 14–25 years [16,40]. Structural wiring models were derived for each subject time point [41], and we estimated longitudinal trajectories in structural network maturation using linear mixed effect models. We assessed whether age-effects on structural wiring were similar to cortical thickness changes in the same subjects [1,11,13,42], and whether wiring changes were consistent after controlling for thickness changes. To study how developmental shifts in structural wiring reflect adolescent functional network maturation, we associated age-effects on structural wiring with those on functional connectivity based on resting-state functional MRI. Multiple sensitivity analyses assessed robustness of our findings with respect to several analysis parameter variations.

RESULTS

We studied 199 healthy participants obtained from the NSPN 2400 cohort, who were part of the accelerated longitudinal design and had imaging data available [16,40]. Included participants had two measurement time points (mean inter-scan interval was 0.94 years, range = 0.5–1), with a mean age of 18.84 (range = 14–25) years at baseline and 19.96 (range = 15–26) years at follow-up. Participants were uniformly distributed across the entire age range, with a similar sex ratio (52/48% males/females). Participant demographics, image processing, and analysis are further detailed in the *Methods*.

Tracking adolescent changes in multiscale cortical wiring

Following a recently developed approach in healthy adults [21], we built cortico-cortical wiring models by combining geodesic distance (GD), microstructural profile covariance (MPC), and tract strength (TS) for every subject time point (**Fig. 1A**). We integrated these three complementary features into a common low-dimensional space using non-linear manifold learning techniques (see *Methods*) [41]. Two eigenvectors (E1, E2) explained approximately 37.8 ± 0.01% (mean ± SD) of information across ten iterations with different non-overlapping subsets within the NSPN cohort (**Fig. 1A–B**; see *Methods*). The first eigenvector (E1) depicted a sensory-fugal gradient, and the second eigenvector (E2) differentiated anterior and posterior cortices.

We calculated Euclidean distance between all brain regions in the wiring-derived manifold space as a measure of wiring differences between them (**Fig. 1C**; see *Methods*). While within-network connectivity showed overall low wiring distance, connections between sensory and transmodal regions showed higher values, indicating overall integration of the nodes involved in the same networks and segregated patterns between networks, sensory and transmodal in particular, in multiscale cortical wiring space. After summarizing node-by-node wiring distance according to functional communities [43], we assessed age-effects on this wiring distance using linear mixed effect models controlling for sex, site, head motion, and subject-specific random intercepts [44]. We found increased wiring distance within ventral attention and default mode networks with advancing age (false discovery rate (FDR) < 0.05; **Fig. 1D**).

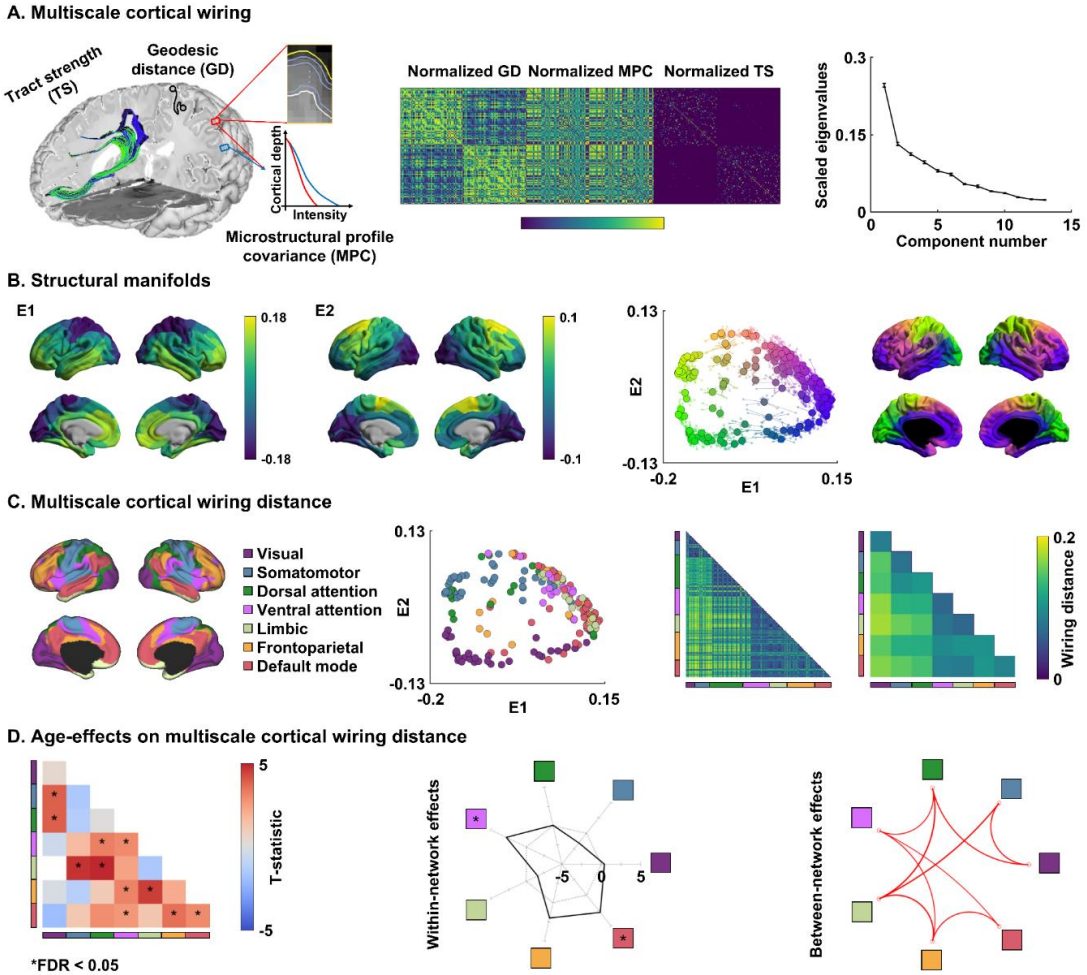

Fig. 1 | Adolescent development of multiscale cortical wiring. (A) Our approach combined three cortical wiring features *i.e.,* geodesic distance (GD), microstructural profile covariance (MPC), and tract strength (TS). Matrices were normalized and concatenated prior to applying non-linear manifold learning, which identifies a coordinate system informed by cortical wiring. The scree plot shows eigenvalues of each estimated component, with error bars indicating the SD across ten repetitions. **(B)** We estimated two eigenvectors (E1, E2) from cortical wiring features. Averaged maps across ten repetitions are reported. The scatter plot represents each brain region projected onto the two-dimensional wiring space with different colors, mapped onto the cortical surface. Solid dots indicate mean across ten repetitions, and transparent dots with lines indicate results from each repetition. **(C)** Nodes in the wiring space were assigned to seven intrinsic functional communities [43]. Multiscale cortical wiring distance, *i.e.,* the Euclidean distance between different nodes in the wiring space, was calculated at a node-level and summarized for intrinsic functional communities. **(D)** The t-statistics of age-effects on cortical wiring distance within- and between-networks are reported, with significant (FDR < 0.05) results marked with asterisks on the lower triangular matrix. The within-network effects are represented with radar plots, and significant networks are reported with asterisks. Significant between-network effects are reported with circular plots. *Abbreviation:* FDR, false discovery rate.

Increases in between-network wiring distance were also observed between nodes of default mode and attention/transmodal regions, as well as between sensory and attention/limbic networks (FDR < 0.05). We additionally assessed age-effects on each cortical feature (*i.e.,* GD, MPC, and TS) to quantify how wiring distance captures age-related changes on cortical organizations relative to change in single features (**Fig. S1**). When analyzing wiring distance, the effect size (*i.e.,* mean of absolute t-statistics across network pairs) was 21.25 ± 12.46% higher than when studying only GD across ten repetitions (see *Methods*), 6.34 ± 5.99% higher than when studying MPC, and 5.49 ± 9.08% higher than when studying TS, indicating that wiring distance describes adolescent cortical reorganization more sensitively than each modality separately. When associating age-effects on wiring distance with those on each feature, wiring distance was strongly related to reductions in MPC (r = -0.75, FDR < 0.001), but not very much to TS (r = -0.11, FDR = 0.58) nor GD (r = 0.003, FDR = 0.99), supporting the

notion that increases in multiscale wiring distance reflected mostly an increased intracortical microstructural differentiation. As the overall manifold size (*i.e.,* mean of wiring distance across all networks) was significantly associated with age ($r = 0.19 \pm 0.02$, $p < 0.001$ across ten repetitions), we repeated linear mixed effect models after additionally controlling for mean wiring distance (**Fig. S2**). Despite decreases in the effect size, we observed overall consistent results, confirming that age-effects on wiring distance were not driven by the expansion in manifold space itself.

Morphological associations

In light of adolescent changes in cortical thickness reported previously [1,11,13,42], we first assessed the similarity of the spatial distribution of age-effects on cortical wiring to age-effects on thickness in our NSPN cohort. As expected, cortical thickness decreased in widespread cortical regions with advancing age (FDR < 0.05; **Fig. 2A**). Thickness effects only showed weak spatial association to changes in wiring measures, with a trend-level association to between-network wiring distance ($r = -0.12 \pm 0.04$ across ten repetitions, spin-test p followed by FDR = 0.06), but not with within-network measure ($r = -0.02 \pm 0.05$, spin-test p followed by FDR = 0.27; **Fig. 2B**). Furthermore, mixed effect models assessed age-effects on wiring distance after controlling for cortical thickness at a node-level. This analysis, thus, examined wiring changes above and beyond morphological changes across age. Importantly, while age-effects on wiring distance within the ventral attention network decreased slightly, patterns remained consistent (**Fig. 2C**). The results suggest that the wiring related changes cannot be just explained by morphological alterations despite subtle spatial similarity of the changes in cortical topography.

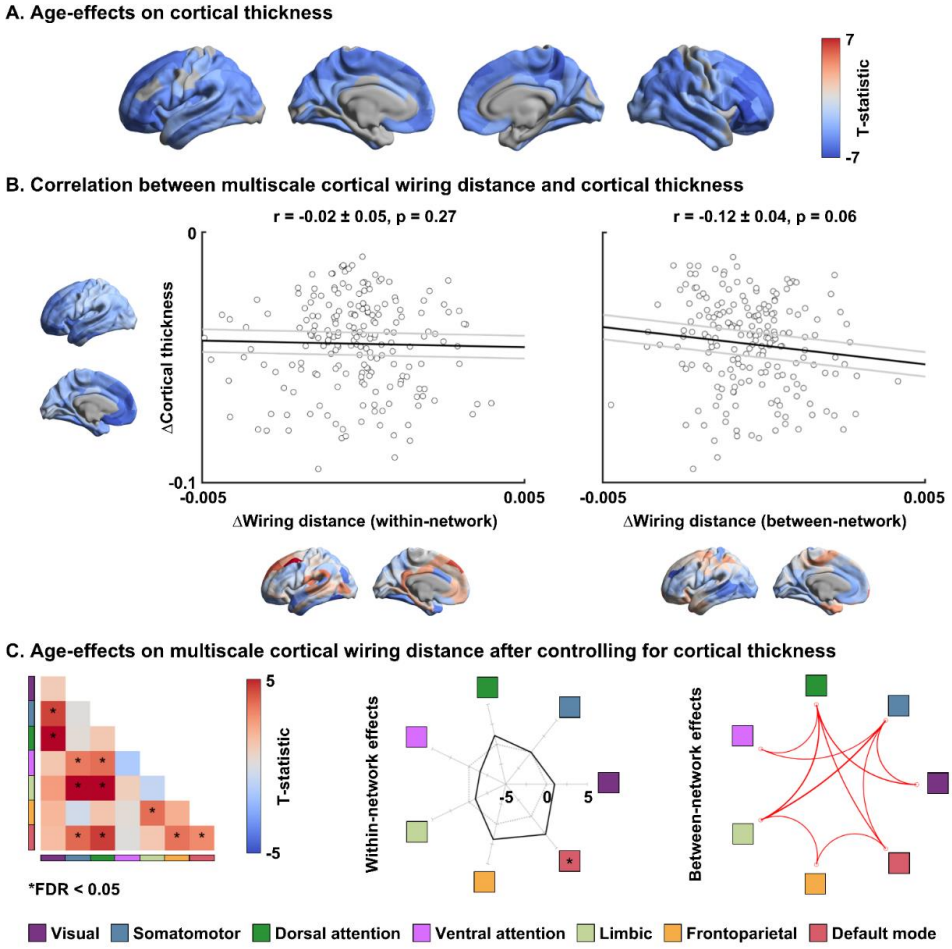

Fig. 2 | Cortical thickness effects. (A) The t-statistics of the identified regions that showed significant (FDR < 0.05) age-related changes in cortical thickness. **(B)** Linear correlations between time-related changes in cortical thickness and

within/between-network wiring distance. **(C)** The t-statistics of age-effects on multiscale cortical wiring distance after controlling for cortical thickness, with significant (FDR < 0.05) results marked with asterisks. The within-network effects are represented with radar plots, and significant networks are reported with asterisks. Significant between-network effects are reported with circular plots. *Abbreviation:* FDR, false discovery rate.

Associations with macroscale functional network maturation

To evaluate functional associations of these changes in multiscale cortical wiring, we first assessed developmental shifts in functional connectivity patterns based on resting-state functional MRI obtained in the same subjects at equivalent time points. When we charted the development of functional connectivity across age, we found decreases in sensory-default mode network connectivity and increases in connectivity between sensory networks (FDR < 0.05; **Fig. 3A**). We then examined associations between structural and functional measures in two ways (**Fig. 3B**). Firstly, we associated structural cortical wiring distance and functional connectivity across intrinsic functional networks at a cross-sectional level and found strong negative structure-function coupling (r = -0.74, spin-test p < 0.001). In other words, regions with increased wiring distance generally show weaker functional connectivity. Secondly, we assessed how the age-related changes in structural and functional measures were inter-related. To this end, we correlated the age-effects on wiring distance controlled for cortical thickness with the age-effects on functional connectivity. Here, we found a tendency for a negative association (r = -0.21, spin-test p = 0.09). The results indicate that cross-sectionally, weaker inter-connectivity in brain function between sensory and transmodal networks is coupled with higher cortical wiring distance between these networks. Moreover, age-related functional differentiation between sensory and default mode networks also tends to be reflected in increased differentiation in structural wiring during adolescence.

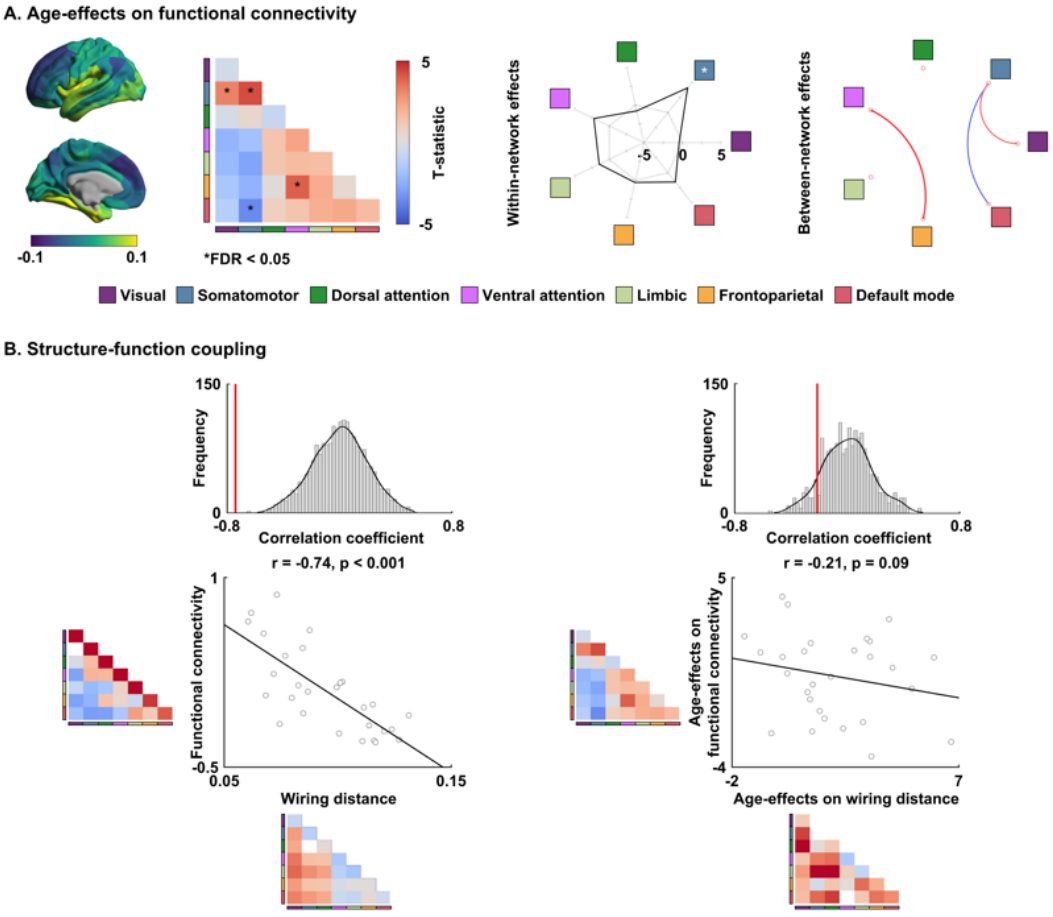

Fig. 3 | Association between functional connectivity and wiring distance. (A) Age-effects on functional connectivity. Spatial maps are represented on brain surfaces, and t-statistics of age-effects are reported. The within-network effects are

represented with radar plots, and significant networks are reported with asterisks. Significant between-network effects are reported with circular plots. **(B)** (left) Cross-sectional and (right) longitudinal structure-function coupling between functional connectivity and cortical wiring distance. Histograms indicate distribution of correlation coefficients, and the actual r-values are represented with red bars. *Abbreviation:* FDR, false discovery rate.

Sensitivity analysis

We assessed whether our findings were robust with respect to several methodological variations.

a) Parcellation scales. We repeated assessing age-effects using different parcellation scales (*i.e.,* 100 and 300 regions) and revealed consistent results (**Fig. S3**), indicating the robustness of our findings across different scales.

b) Structural manifold generation using principal component analysis. Our main analysis estimated structural manifolds using diffusion map embedding [45], in keeping with a previous approach to study structural manifolds in healthy young adults [21,46]. We repeated our analysis after alternatively estimating structural manifolds using principal component analysis [47], and the manifolds and age-effects were similar (**Fig. S4**), confirming robustness.

c) Parcellation scheme. We generated connectome manifolds and assessed adolescent remodeling using a functional (*i.e.,* Schaefer) parcellation [48] instead of structural parcellation scheme [49], and found consistent results (**Fig. S5**), indicating the robustness of our analyses across different parcellations.

DISCUSSION

The current work longitudinally assessed adolescent maturation of cortical networks based on a comprehensive *in vivo* model that encompasses several dimensions of cortical wiring within a compact coordinate system [21]. Charting typical development from late childhood to early adulthood longitudinally, we observed marked increases in within- and between-network wiring distances in both sensory and transmodal association networks. Findings occurred rather independently of parallel changes in MRI-based cortical thickness measures, suggesting that cortical wiring changes occurred above and beyond commonly observed morphological maturation. Moreover, associating cortical structural wiring features with intrinsic functional connectivity obtained in the same subjects, we observed that functional network reconfigures in parallel with structural reorganization. Collectively, our work offers a novel perspective on how structural brain networks reconfigure during typical adolescence and how these changes give rise to ongoing functional maturation.

Our work centered on a comprehensive model of structural wiring that integrated multiple dimensions of cortico-cortical connectivity [21], namely diffusion MRI tractography strength (TS), geodesic distance (GD), and microstructure profile covariance (MPC). Each feature taps into different aspects of structural wiring, grounded in seminal neuroanatomical work on the multiple facets of the cortical wiring scheme [50]. Synergistic integration of these features is hypothesized to comprehensively describe structural connectivity, and to thus shine a light into structure-function relationships in the developing brain. In fact, TS is an established measure of short- and long-range fibers in the white matter [51,52], whereas GD is computed within the cortical ribbon, approximating horizontal connectivity between adjacent cortical regions [24,53]. Similarity of intracortical microstructural profiles, quantified as MPC [28], is also recognized as an indicator of inter-regional connectivity [21,27,54,55]. In fact, the structural model of brain connectivity formulated in non-human animals predicts that areas with similar microstructure are more likely to be connected than areas with different connectivity profiles [56]. These findings were recently expanded to *in vivo* human

neuroanatomy by relating microstructural similarity to diffusion MRI-derived streamline strength [55,57] and to resting-state functional connectivity [28,58]. Here, we fused and mapped the three above cortical wiring features into a 2D coordinate system using manifold learning techniques [21,41,45]. By translating this approach previously formulated in adults [21] to adolescents, we demonstrated that the wiring space in youth overall resembles the one previously seen in adults. Indeed, the two principal dimensions of the wiring space represented sensory-fugal and anterior-posterior gradients – both major axes of adult macroscale cortical topography [59–63]. On the other hand, we could obtain new insights into adolescent reconfigurations of structural networks via longitudinal analyses. The NSPN dataset follows an accelerated longitudinal design ranging from late childhood to young adulthood [16,40]. Compared to cross-sectional studies, longitudinal designs measure intra-individual changes in cortical features and chart developmental trajectories directly [3,20,64–66]. Our multiscale approach gathered evidence for developmental shifts in cortical wiring, indicative of increased wiring distances in multiple systems of the cortical mantle, with highest effects in default mode and ventral attention networks. These findings indicate a continued differentiation of cortico-cortical structural networks, which most markedly take place in transmodal systems at the apex of the cortical hierarchy [3,37,67,68]. Notably, wiring space analysis revealed increased effects compared to analysis of single features, suggesting that our compact multiscale approach may offer additional sensitivity in the study of adolescent development. These findings could thus recapitulate prior work in adolescence more generally and the NSPN dataset specifically, including our recent work showing overall changes in cortical myelination [16,69] as well as depth-dependent shifts in intracortical myeloarchitecture [17]. Moreover, several studies have described structural connectivity changes based on diffusion MRI tractography, reporting general increases in streamline strength in transmodal areas in adolescence [20,70], together with enhanced within-module integration and strengthening of structural hubs, sometimes alongside a weakening of more local connections [71,72]. In our work, different constituent wiring features contributed in a graded manner to our overall findings, with a marked association wiring distance increases and ongoing microstructural differentiation of transmodal areas from the rest of the brain [17].

Alterations in cortical morphology during adolescence are well established, and the prevailing findings in literature indicate widespread cortical thickness reductions with advancing age, a finding likely reflecting ongoing synaptic pruning and cortical myelination [10,16,73,74]. Here, by analyzing longitudinal cortical thickness changes in the same NSPN participants, we could confirm widespread cortical thinning in youth with advancing age. What's more, we showed that wiring space changes were only partially attributable to these changes in cortical thickness, despite subtle resemblances in the overall spatial distribution of findings, suggesting that age-related structural wiring changes likely occurred above and beyond maturational effects on cortical morphology per se. In prior work in healthy adults [21], we could identify associations between *in vivo* cortical wiring space organization and intracortical factors, specifically cell-type specific gene expression as well as externopyramidization. Although these associations were indirect and based on separate datasets (*in vivo* MRI and histology-based *post mortem* gene expression information), they nevertheless supported a link between multiscale wiring and internal cortical microcircuitry that go beyond the changes measurable by cortical thickness measures alone. Such interactions between different scales of cortical organization during typical development could be further explored in studies obtaining wiring space data and gene expression in the same subjects or model systems.

During adolescence, the age-related reconfiguration in functional connectome organization has recently been shown to mainly follow two distinct trajectories, labeled as conservative and disruptive modes [37]. Conservative modes involve the ongoing strengthening of already strong functional connectivity and primarily take place in primary cortical regions. On the other hand, disruptive functional maturational trajectories have been observed in cortical association areas and subcortical nodes, and are characterized by a strengthening of initially weak connections or as a weakening of initially strong connections [37]. These results complement our structural wiring space findings of an

alteration of functional network topologies in adolescence, which showed increases in wiring distance between sensory and transmodal regions. Furthermore, assessing spatial associations between age-effects on structural wiring and functional connectivity, we observed that adolescent decreases in functional connectivity between sensory and association systems are marginally reflected in increased cortical wiring distances between these systems. These segregation patterns of sensory-transmodal networks echo prior studies in individuals aged 8-23 that has shown marked reconfigurations of structure-function coupling during development, particularly in sensory and transmodal regions, which further could support increased functional flexibility and cognitive control with advancing age during that time window [3,38,75].

To conclude, we utilized a comprehensive model of cortical structural wiring and showed continued shifts in multiple brain networks in adolescence. Despite subtle spatial resemblance, wiring changes were relatively independent of changes in cortical morphology that co-occur in this time window. On the other hand, functional network trajectories occurred alongside structural wiring reconfigurations. Our multimodal framework, thus, provides novel insights into the coordination of structural and functional brain development in adolescence across multiple spatial scales.

METHODS

Participants

We obtained imaging and phenotypic data from the NSPN 2400 cohort, which contains questionnaire data on 2,402 individuals (with MRI data in a subset of ~300) from adolescence to young adulthood in a longitudinal setting [16,40]. In this study, we included 199 participants who completed quality-controlled (see *Data preprocessing* section) multimodal MRI scans consisting of T1-weighted, magnetization transfer (MT), diffusion MRI, and resting-state functional MRI for at least two time points (48% female; mean ± SD age = 18.84 ± 2.83 (between 14 and 25) years at baseline and 19.96 ± 2.84 (between 15 and 26) years at follow-up with inter-scan interval of 0.94 ± 0.17 (between 0.5 and 1) years). Data were collected from three different sites: Wolfson Brain Imaging Centre; MRC Cognition and Brain Sciences Unit in Cambridge; and University College London. Participants provided informed written consent for each aspect of the study, and parental consent was obtained for those aged 14–15 years old. Ethical approval was granted for this study by the NHS NRES Committee East of England-Cambridge Central (project ID 97546). The authors assert that all procedures contributing to this work comply with the ethical standards of the relevant national and institutional committees on human experimentation and with the Helsinki Declaration of 1975, as revised in 2008.

MRI acquisition

Imaging data were obtained using a Siemens Magnetom TIM Trio 3T scanner at all sites. The T1-weighted and MT sequences were acquired using a quantitative multiparameter mapping (MPM) sequence (repetition time (TR)/flip angle = 18.7ms/20º for T1-weighted and 23.7ms/6º for MT; six equidistance echo times (TE) = 2.2–14.7ms; voxel size = 1mm^3; 176 slices; field of view (FOV) = 256 × 240mm; matrix size = 256 × 240 × 176) [76]. The diffusion MRI data were acquired using a spin-echo echo-planar imaging (EPI) sequence (TR = 8,700ms; TE = 90ms; flip angle = 90º; voxel size = 2mm^3; 70 slices; FOV = 192 × 192mm^2; matrix size = 96 × 96 × 70; b-value = 1,000s/mm^2; 63 diffusion directions; and 6 b0 images). The resting-state functional MRI data were collected using a multi-echo EPI sequence with three different TEs (TR = 2.43 ms; TE = 13.0/30.55/48.1 ms; flip angle = 90º; voxel size = 3.75 × 3.75 × 4.18 mm^3; 34 slices; FOV = 240 × 240 mm^2; matrix size = 64 × 64 × 34; and 269 volumes).

Data preprocessing

T1-weighted data were processed using the fusion of neuroimaging preprocessing (FuNP) pipeline integrating AFNI, FSL, FreeSurfer, ANTs, and Workbench (https://gitlab.com/by9433/funp) [77–81], which is similar to the minimal preprocessing pipeline for the Human Connectome Project [82]. Gradient nonlinearity and b0 distortion correction, non-brain tissue removal, and intensity normalization were performed. The white and pial surfaces were generated by following the boundaries between different tissues [79,83–85]. The midthickness surface was generated by averaging the white and pial surfaces, and it was used to generate an inflated surface. Quality control involved visual inspection of surface reconstruction of T1-weighted data, and cases with faulty cortical segmentation were excluded. Surface-based co-registration between T1-weighted and MT weighted scans were performed. We generated 14 equivolumetric cortical surfaces within the cortex, especially between inner white and outer pial surfaces, and sampled MT intensity along these surfaces [28]. The diffusion MRI data were processed using MRtrix3 [23], including correction for susceptibility distortions, head motion, and eddy currents. The resting-state functional MRI data were processed using multi-echo independent component analysis (ME-ICA) pipeline (https://github.com/ME-ICA/me-ica) [86,87]. The first six volumes were discarded to allow for the magnetic field saturation, and slice timing was corrected. Motion correction parameters were estimated from the middle TE data by aligning all volumes to the first volume using rigid-body transformation. The co-registration transformation parameters from functional to structural image were estimated by registering the skull-stripped spatially concatenated multi-echo functional data to the skull-stripped anatomical image using affine transformation. The estimated motion correction and anatomical co-registration parameters were applied to each slice-timing corrected TE data and then temporally concatenated. The noise components were removed using principal component analysis followed by independent component analysis [86,87]. The processed functional MRI data were mapped to the standard grayordinate space (*i.e.,* 32k Conte69) with a cortical ribbon-constrained volume-to-surface mapping algorithm. Finally, data were surface smoothed with 5 mm full width at half maximum.

Multiscale cortical wiring features

We calculated complementary cortical wiring features from different imaging sequences, namely GD from T1-weighted, MPC from MT, and TS from diffusion MRI (**Fig. 1A**). GD is a physical distance represented by the shortest paths between two points along the cortical surface [24,46,53]. To calculate the GD matrix, we first matched each vertex to the nearest voxel in volume space. Then we calculated the distance to all other voxels traveling through a grey/white matter mask using a Chamfer propagation (https://github.com/mattools/matImage/wiki/imGeodesics) [88]. Unlike a previously introduced approach that calculates only intra-hemispheric distance [24,46,53], this approach allows estimating interhemispheric projections [21]. We mapped GD to 200 cortical nodes parcellation scheme, which preserves the boundaries of the Desikan Killiany atlas [49]. Following our prior study in adults [28], the MPC matrix was constructed by calculating linear correlation of cortical depth-dependent intensity profiles between different nodes, controlling for the average whole-cortex intensity profile based on the 200 parcels. The MPC matrix was thresholded at zero and log-transformed. We generated the TS matrix from preprocessed diffusion MRI data using MRtrix3 [23]. Anatomical constrained tractography was performed using different tissue types derived from the T1-weighted image, including cortical and subcortical grey matter, white matter, and cerebrospinal fluid [89]. We estimated co-registration transformation from T1-weighted to diffusion MRI data with boundary-based registration and applied the transformation to different tissue types to align them onto the native diffusion MRI space. The multi-shell and multi-tissue response functions were estimated [90], and constrained spherical deconvolution and intensity normalization were performed [91]. Seeding from all white matter voxels, the tractogram was generated using a probabilistic approach

[23,92] with 40 million streamlines, a maximum tract length of 250, and a fractional anisotropy cutoff of 0.06. Subsequently, we applied spherical-deconvolution informed filtering of tractograms (SIFT2) to optimize an appropriate cross-section multiplier for each streamline [93], and reconstructed whole-brain streamlines weighted by cross-section multipliers. Reconstructed cross-section streamlines were mapped onto the 200 parcels to build TS matrix, and log-transformed [94,95].

Structural manifold identification

We estimated structural manifolds based on the multiscale cortical features calculated above using an openly accessible normative manifold map approach (https://github.com/MICA-MNI/micaopen/tree/master/structural_manifold) [21], which is now integrated in BrainSpace (https://github.com/MICA-MNI/BrainSpace) [41]. First, we rank normalized nonzero entries of the input matrices, and the less sparse matrices (*i.e.,* GD and MPC) were rescaled to the same numerical range as the sparsest matrix (*i.e.,* TS) to balance the contribution of each input measure (**Fig. 1A**). Notably, we rank normalized the inverted GD matrix to represent closer regions with larger values. We horizontally concatenated the normalized GD, MPC, and TS matrices and constructed an affinity matrix with a normalized angle kernel with 10% density, which quantifies the strength of cortical wiring between two regions. Structural manifolds were estimated via diffusion map embedding [45] (**Fig. 1B**), which is robust to noise and computationally efficient compared to other non-linear manifold learning techniques [96,97]. It is controlled by two parameters α and t, where α controls the influence of the density of sampling points on the manifold ($\alpha = 0$, maximal influence; $\alpha = 1$, no influence) and t controls the scale of eigenvalues of the diffusion operator. We set $\alpha = 0.5$ and $t = 0$ to retain the global relations between data points in the embedded space, following prior applications [17,20,28,41,46,98,99]. Cortical regions with more similar inter-regional patterns are more proximal in this new structural manifold. To assess robustness, we repeated estimating structural manifolds ten times with different sets of participants. Specifically, we split the dataset into non-overlapping template (1/10) and non-template (9/10) partitions with similar distribution of age, sex, and site. The template manifold was generated using the averaged concatenated matrix of template dataset, and individual-level manifolds were estimated from the non-template dataset and aligned to the template manifold via Procrustes alignment [41,100]. We repeated generating connectome manifolds ten times with different template and non-template datasets.

Age-effects on structural manifolds

To chart age-effects on structural manifolds, we first calculated multiscale cortical wiring distance, which is the Euclidean distance between different brain regions in the manifold space (**Fig. 1C**) [21,101]. We stratified the node-level wiring distance based on intrinsic functional communities [43] and assessed age-effects on network-level wiring distance using a linear mixed effect model [44]. The model additionally controlled for sex, site, head motion (*i.e.,* frame-wise displacement measured from diffusion MRI), and included a subject-specific random intercept. We corrected for multiple comparisons across all pairs of functional communities with FDR < 0.05 [102]. We repeated the age modeling ten times with different non-template individuals and reported only those network pairs showing significant effects across all repetitions (**Fig. 1D**). We additionally implemented mixed effect models for each cortical wiring feature separately (*i.e.,* GD, MPC, and TS) to assess how much the age-effects improved when we considered multiscale cortical wiring distance (**Fig. S1**). The age-effect t-statistics of each feature were correlated with those of wiring distance to assess which features are strongly related to adolescent development in wiring distance. To assess the association between global manifold effects and age, we calculated linear correlation between age and mean wiring distance across the whole network. We also implemented a linear mixed effect model that additionally controlled for mean wiring distance to assess whether the age-effects on wiring distance are affected by global changes in the size of manifold space (**Fig. S2**).

Association with cortical thickness

It has been shown that cortical thickness shows significant changes across age [1,11,13,42]. We first replicated these morphological findings by assessing age-effects on cortical thickness measured using T1-weighted MRI (**Fig. 2A**). Next, we linearly correlated time-related changes in wiring distance and those in cortical thickness to assess spatial similarity across the cortex (**Fig. 2B**). The significance of the similarity was assessed based on 1,000 spin tests that account for spatial autocorrelation [41,103], and FDR corrected across within and between-network correlations. We then implemented the linear mixed effect model using the wiring distance controlled for cortical thickness to assess whether the effects are independent of the cortical thickness maturation (**Fig. 2C**). We repeated these analyses ten times with different non-template individuals, and only the network pairs that showed consistent results across repetitions were reported.

Association between structural manifolds and functional connectivity

Structure-function coupling analyses assessed how age-effects on multiscale cortical wiring related to functional connectivity. First, we constructed the functional connectivity matrix by calculating linear correlations of resting-state functional time series between different brain regions, controlling for average whole-cortex signals. After row-wise thresholding remaining 10% of values for each row in the connectivity matrix, assessed age-effects on z-transformed functional connectivity to obtain node by node t-statistics (**Fig. 3A**). Then, we assessed structure-function correspondence by computing linear correlations between the functional connectivity and wiring distance, as well as age-effect t-statistics of each measure (**Fig. 3B**). We calculated correlations 1,000 times with spin test [41,103].

Sensitivity analysis

a) Parcellation scales. Our main analyses were based on the structural atlas of 200 cortical nodes defined using Desikan Killiany atlas [49]. To assess robustness across multiple parcellation scales, we generated structural manifolds using structural atlases with 100 and 300 parcels and repeated the age modeling (**Fig. S3**).

b) Structural manifold generation using principal component analysis. Instead of relying on diffusion map embedding [45], we generated structural manifolds using principal component analysis [47]. Then, we repeated calculating multiscale cortical wiring distance and assessed age-effects to evaluate consistency of our findings (**Fig. S4**).

c) Functional parcellation. We also repeated structural manifold generation and age modeling using the functional Schaefer parcellation scheme with 200 parcels [48] (**Fig. S5**).

DATA AND CODE AVAILABILITY

The imaging and phenotypic data were provided by the Neuroscience in Psychiatry Network (NSPN) 2400 cohort. As stated in https://doi.org/10.1093/ije/dyx117, the NSPN project is committed to make the anonymised dataset fully available to the research community, and participants have consented to their de-identified data being made available to other researchers. A data request can be made to openNSPN@medschl.cam.ac.uk. Codes for multimodal connectome manifold generation are provided at https://github.com/MICA-MNI/micaopen/tree/master/structural_manifold and https://github.com/MICA-MNI/BrainSpace, and those for wiring distance calculation are provided at https://github.com/MICA-MNI/micaopen/tree/master/manifold_features.

ACKNOWLEDGMENTS

Dr. Bo-yong Park was funded by the National Research Foundation of Korea (NRF-2021R1F1A1052303), Institute for Information and Communications Technology Planning and Evaluation (IITP) funded by the Korea Government (MSIT) (2020-0-01389, Artificial Intelligence Convergence Research Center, Inha University), and Institute for Basic Science (IBS-R015-D1). Dr. Richard A. I. Bethlehem was funded by a British Academy Post-Doctoral Fellowship and the Autism Research Trust. Dr. Edward T. Bullmore was supported by a Senior Investigator award from the National Institute of Health Research (NIHR). Dr. Boris C. Bernhardt acknowledges research support from the National Science and Engineering Research Council of Canada (NSERC Discovery-1304413), CIHR (FDN-154298, PJT-174995), SickKids Foundation (NI17-039), Azrieli Center for Autism Research (ACAR-TACC), BrainCanada (Azrieli Future Leaders), and the Tier-2 Canada Research Chairs program. The Neuroscience and Psychiatry Network (NSPN) study was funded by a Wellcome Trust award to the University of Cambridge and University College London. The data were curated and analyzed using a computational facility funded by an MRC research infra-structure award (MR/M009041/1) and supported by the NIHR Cambridge Biomedical Research Centre. The views expressed are those of the authors and not necessarily those of the NHS, the NIHR or the Department of Health and Social Care.

AUTHOR CONTRIBUTIONS

B.P. and B.C.B. designed the experiments, analyzed the data, and wrote the manuscript. C.P. and O.B. aided with the experiments. R.A.I.B. aided data curation. E.T.B. designed the NSPN MRI study. C.P., R.A.I.B., B.M., J.S., and E.T.B. reviewed and edited the manuscript. B.P. and B.C.B. are the corresponding authors of this work and have responsibility for the integrity of the data analysis.

CONFLICT OF INTEREST

E.T.B. serves on the scientific advisory board of Sosei Heptares and as a consultant for GlaxoSmithKline. Other authors declare no conflicts of interest.

REFERENCES

1. Shaw P, Greenstein D, Lerch J, Clasen L, Lenroot R, Gogtay N, et al. Intellectual ability and cortical development in children and adolescents. Nature. 2006;440: 676–679. doi:10.1038/nature04513

2. Gogtay N, Giedd JN, Lusk L, Hayashi KM, Greenstein D, Vaituzis AC, et al. Dynamic mapping of human cortical development during childhood through early adulthood. Proc Natl Acad Sci U S A. 2004;101: 8174–8179. doi:10.1073/pnas.0402680101

3. Baum GL, Cui Z, Roalf DR, Ciric R, Betzel RF, Larsen B, et al. Development of structure–function coupling in human brain networks during youth. Proc Natl Acad Sci U S A. 2020;117: 771–778. doi:10.1073/pnas.1912034117

4. Dwyer DB, Harrison BJ, Yücel M, Whittle S, Zalesky A, Pantelis C, et al. Large-scale brain network dynamics supporting adolescent cognitive control. J Neurosci. 2014;34: 14096–14107. doi:10.1523/JNEUROSCI.1634-14.2014

5. Menon V. Developmental pathways to functional brain networks: Emerging principles. Trends Cogn Sci. 2013;17: 627–640. doi:10.1016/j.tics.2013.09.015

6. Kolskår KK, Alnæs D, Kaufmann T, Richard G, Sanders AM, Ulrichsen KM, et al. Key brain network nodes show differential cognitive relevance and developmental trajectories during childhood and adolescence. eNeuro. 2018;5. doi:10.1523/ENEURO.0092-18.2018

7. Larsen B, Luna B. Adolescence as a neurobiological critical period for the development of higher-order cognition. Neurosci Biobehav Rev. 2018;94: 179–195. doi:10.1016/j.neubiorev.2018.09.005

8. Paus T, Keshavan M, Giedd JN. Why do many psychiatric disorders emerge during adolescence? Nat Rev Neurosci. 2008;9: 947–957. doi:10.1038/nrn2513

9. Casey BJ, Jones RM, Hare TA. The adolescent brain. Ann N Y Acad Sci. 2008;1124: 111–126. doi:10.1196/annals.1440.010

10. Giedd JN, Blumenthal J, Jeffries NO, Castellanos FX, Liu H, Zijdenbos A, et al. Brain development during childhood and adolescence: A longitudinal MRI study. Nat Neurosci. 1999;10: 861–863.

11. Sotiras A, Toledo JB, Gur RE, Gur RC, Satterthwaite TD, Davatzikos C. Patterns of coordinated cortical remodeling during adolescence and their associations with functional specialization and evolutionary expansion. Proc Natl Acad Sci U S A. 2017;114: 3527–3532. doi:10.1073/pnas.1620928114

12. Hill J, Inder T, Neil J, Dierker D, Harwell J, Van Essen D. Similar patterns of cortical expansion during human development and evolution. Proc Natl Acad Sci U S A. 2010;107: 13135–13140. doi:10.1073/pnas.1001229107

13. Tamnes CK, Herting MM, Goddings AL, Meuwese R, Blakemore SJ, Dahl RE, et al. Development of the cerebral cortex across adolescence: A multisample study of inter-related longitudinal changes in cortical volume, surface area, and thickness. J Neurosci. 2017;37: 3402–3412. doi:10.1523/JNEUROSCI.3302-16.2017

14. Raznahan A, Greenstein D, Lee NR, Clasen LS, Giedd JN. Prenatal growth in humans and postnatal brain maturation into late adolescence. Proc Natl Acad Sci U S A. 2012;109: 11366–11371. doi:10.1073/pnas.1203350109

15. Miller DJ, Duka T, Stimpson CD, Schapiro SJ, Baze WB, McArthur MJ, et al. Prolonged myelination in human neocortical evolution. Proc Natl Acad Sci U S A. 2012;109: 16480–16485. doi:10.1073/pnas.1117943109

16. Whitaker KJ, Vértes PE, Romero-Garciaa R, Váša F, Moutoussis M, Prabhu G, et al. Adolescence is associated with genomically patterned consolidation of the hubs of the human brain connectome. Proc Natl Acad Sci U S A. 2016;113: 9105–9110. doi:10.1073/pnas.1601745113

17. Paquola C, Bethlehem RA, Seidlitz J, Wagstyl K, Romero-Garcia R, Whitaker KJ, et al. Shifts in myeloarchitecture characterise adolescent development of cortical gradients. Elife. 2019;8: e50482. doi:10.7554/eLife.50482

18. Dosenbach NUF, Nardos B, Cohen AL, Fair DA, Power JD, Church JA, et al. Prediction of individual brain maturity using fMRI. Science (80-). 2010;329: 1358–1361. doi:10.1126/science.1194144

19. Fair DA, Cohen AL, Power JD, Dosenbach NUF, Church JA, Miezin FM, et al. Functional brain networks develop from a “local to distributed” organization. PLoS Comput Biol. 2009;5: 14–23. doi:10.1371/journal.pcbi.1000381

20. Park B, Bethlehem RAI, Paquola C, Larivière S, Rodríguez-Cruces R, Vos de Wael R, et al. An expanding manifold in transmodal regions characterizes adolescent reconfiguration of structural connectome organization. Elife. 2021;10: e64694. doi:10.7554/eLife.64694

21. Paquola C, Seidlitz J, Benkarim O, Royer J, Klimes P, Bethlehem RAI, et al. A multi-scale cortical wiring space links cellular architecture and functional dynamics in the human brain. PLoS Biology. 2020. doi:10.1371/journal.pbio.3000979

22. Tournier JD, Calamante F, Connelly A. MRtrix: Diffusion tractography in crossing fiber regions. Int J Imaging Syst Technol. 2012;22: 53–66. doi:10.1002/ima.22005

23. Tournier JD, Smith R, Raffelt D, Tabbara R, Dhollander T, Pietsch M, et al. MRtrix3: A fast, flexible and open software framework for medical image processing and visualisation. Neuroimage. 2019;202: 116137. doi:10.1016/j.neuroimage.2019.116137

24. Ecker C, Ronan L, Feng Y, Daly E, Murphy C, Ginestet CE, et al. Intrinsic gray-matter connectivity of the brain in adults with autism spectrum disorder. Proc Natl Acad Sci U S A. 2013;110: 13222–13227. doi:10.1073/pnas.1221880110

25. Alexander-Bloch A, Raznahan A, Bullmore E, Giedd J. The convergence of maturational change and structural covariance in human cortical networks. J Neurosci. 2013;33: 2889–2899. doi:10.1523/JNEUROSCI.3554-12.2013

26. Alexander-Bloch A, Giedd JN, Bullmore E. Imaging structural co-variance between human brain regions. Nat Rev Neurosci. 2013;14: 322–336. doi:10.1038/nrn3465

27. Barbas H, Rempel-Clower N. Cortical structure predicts the pattern of corticocortical connections. Cereb Cortex. 1997;7: 635–646. doi:10.1093/cercor/7.7.635

28. Paquola C, Vos De Wael R, Wagstyl K, Bethlehem RAI, Hong SJ, Seidlitz J, et al. Microstructural and functional gradients are increasingly dissociated in transmodal cortices. PLoS Biol. 2019;17: e3000284. doi:10.1371/journal.pbio.3000284

29. Batista-García-Ramó K, Fernández-Verdecia CI. What we know about the brain structure-function relationship. Behav Sci (Basel). 2018;8: 39. doi:10.3390/bs8040039

30. Honey CJ, Sporns O, Cammoun L, Gigandet X, Thiran JP, Meuli R, et al. Predicting human resting-state functional connectivity from structural connectivity. Proc Natl Acad Sci U S A. 2009;106: 2035–2040. doi:10.1073/pnas.0811168106

31. Mišic B, Betzel RF, De Reus MA, Van Den Heuvel MP, Berman MG, McIntosh AR, et al. Network-level structure-function relationships in human neocortex. Cereb Cortex. 2016;26: 3285–3296. doi:10.1093/cercor/bhw089

32. Park HJ, Friston K. Structural and functional brain networks: From connections to cognition. Science (80-). 2013;342: 1238411. doi:10.1126/science.1238411

33. Suárez LE, Markello RD, Betzel RF, Misic B. Linking Structure and Function in Macroscale Brain Networks. Trends Cogn Sci. 2020;24: 302–315. doi:10.1016/j.tics.2020.01.008

34. Wang Z, Dai Z, Gong G, Zhou C, He Y. Understanding structural-functional relationships in the human brain: A large-scale network perspective. Neuroscientist. 2015;21: 290–305. doi:10.1177/1073858414537560

35. Park B, Vos de Wael R, Paquola C, Larivière S, Benkarim O, Royer J, et al. Signal diffusion along connectome gradients and inter-hub routing differentially contribute to dynamic human brain function. Neuroimage. 2021;224: 117429. doi:10.1016/j.neuroimage.2020.117429

36. Kundu P, Benson BE, Rosen D, Frangou S, Leibenluft E, Luh WM, et al. The integration of functional brain activity from adolescence to adulthood. J Neurosci. 2018;38: 3559–3570. doi:10.1523/JNEUROSCI.1864-17.2018

37. Váša F, Romero-Garcia R, Kitzbichler MG, Seidlitz J, Whitaker KJ, Vaghi MM, et al. Conservative and disruptive modes of adolescent change in human brain functional connectivity. Proc Natl Acad Sci U S A. 2020;117: 3248–3253. doi:10.1073/pnas.1906144117

38. Baum GL, Ciric R, Roalf DR, Betzel RF, Moore TM, Shinohara RT, et al. Modular Segregation of Structural Brain Networks Supports the Development of Executive Function in Youth. Curr Biol. 2017;27: 1561-1572.e8. doi:10.1016/j.cub.2017.04.051

39. Esfahlani FZ, Faskowitz J, Slack J, Miˇ B. Local structure-function relationships in human brain networks across the human lifespan. bioRxiv. 2021. doi:10.1101/2021.05.23.445128

40. Kiddle B, Inkster B, Prabhu G, Moutoussis M, Whitaker KJ, Bullmore ET, et al. Cohort profile: The NSPN 2400 Cohort: A developmental sample supporting the Wellcome Trust Neuro Science in Psychiatry Network. Int J Epidemiol. 2018;47: 18-19g. doi:10.1093/ije/dyx117

41. Vos de Wael R, Benkarim O, Paquola C, Lariviere S, Royer J, Tavakol S, et al. BrainSpace: a toolbox for the analysis of macroscale gradients in neuroimaging and connectomics datasets. Commun Biol. 2020;3: 103. doi:10.1038/s42003-020-0794-7

42. Khundrakpam BS, Reid A, Brauer J, Carbonell F, Lewis J, Ameis S, et al. Developmental changes in organization of structural brain networks. Cereb Cortex. 2013;23: 2072–2085. doi:10.1093/cercor/bhs187

43. Yeo BTT, Krienen FM, Sepulcre J, Sabuncu MR, Lashkari D, Hollinshead M, et al. The organization of the human cerebral cortex estimated by intrinsic functional connectivity. J Neurophysiol. 2011;106: 1125–1165. doi:10.1152/jn.00338.2011.

44. Worsley KJ, Taylor JE, Carbonell, Chung MK, Duerden E, Bernhardt B, et al. SurfStat: A Matlab toolbox for the statistical analysis of univariate and multivariate surface and

volumetric data using linear mixed effects models and random field theory. Neuroimage. 2009;47: S102. doi:10.1016/S1053-8119(09)70882-1

45. Coifman RR, Lafon S. Diffusion maps. Appl Comput Harmon Anal. 2006;21: 5–30. doi:10.1016/j.acha.2006.04.006

46. Margulies DS, Ghosh SS, Goulas A, Falkiewicz M, Huntenburg JM, Langs G, et al. Situating the default-mode network along a principal gradient of macroscale cortical organization. Proc Natl Acad Sci U S A. 2016;113: 12574–12579. doi:10.1073/pnas.1608282113

47. Wold S, Esbensen K, Geladi P. Principal component analysis. Chemom Intell Lab Syst. 1987;2: 37–52. doi:10.1016/0169-7439(87)80084-9

48. Schaefer A, Kong R, Gordon EM, Laumann TO, Zuo X-N, Holmes AJ, et al. Local-Global Parcellation of the Human Cerebral Cortex from Intrinsic Functional Connectivity MRI. Cereb Cortex. 2018;28: 3095–3114. doi:10.1093/cercor/bhx179

49. Desikan RS, Ségonne F, Fischl B, Quinn BT, Dickerson BC, Blacker D, et al. An automated labeling system for subdividing the human cerebral cortex on MRI scans into gyral based regions of interest. Neuroimage. 2006;31: 968–980. doi:10.1016/j.neuroimage.2006.01.021

50. Braitenberg V, Schüz A. Anatomy of the Cortex. 1991.

51. Sotiropoulos SN, Zalesky A. Building connectomes using diffusion MRI: why, how and but. NMR Biomed. 2019;32: e3752. doi:10.1002/nbm.3752

52. Reveley C, Seth AK, Pierpaoli C, Silva AC, Yu D, Saunders RC, et al. Superficial white matter fiber systems impede detection of long-range cortical connections in diffusion MR tractography. Proc Natl Acad Sci U S A. 2015;112: E2820–E2828. doi:10.1073/pnas.1418198112

53. Hong SJ, Valk SL, Di Martino A, Milham MP, Bernhardt BC. Multidimensional neuroanatomical subtyping of autism spectrum disorder. Cereb Cortex. 2018;28: 3578–3588. doi:10.1093/cercor/bhx229

54. García-Cabezas MÁ, Zikopoulos B, Barbas H. The Structural Model: a theory linking connections, plasticity, pathology, development and evolution of the cerebral cortex. Brain Struct Funct. 2019;224: 985–1008. doi:10.1007/s00429-019-01841-9

55. Wei Y, Scholtens LH, Turk E, van den Heuvel MP. Multiscale examination of cytoarchitectonic similarity and human brain connectivity. Netw Neurosci. 2019;3: 124–137. doi:10.1162/netn_a_00057

56. Delettre C, Messé A, Dell LA, Foubet O, Heuer K, Larrat B, et al. Comparison between diffusion MRI tractography and histological tract-tracing of cortico-cortical structural connectivity in the ferret brain. Netw Neurosci. 2019;3: 1038–1050. doi:10.1162/netn_a_00098

57. Wahl M, Li YO, Ng J, LaHue SC, Cooper SR, Sherr EH, et al. Microstructural correlations of white matter tracts in the human brain. Neuroimage. 2010;51: 531–541. doi:10.1016/j.neuroimage.2010.02.072

58. Huntenburg JM, Bazin PL, Margulies DS. Large-Scale Gradients in Human Cortical Organization. Trends in Cognitive Sciences. 2018. pp. 21–31. doi:10.1016/j.tics.2017.11.002

59. Badre D, D'Esposito M. Is the rostro-caudal axis of the frontal lobe hierarchical? Nat Rev Neurosci. 2009;10: 659–669. doi:10.1038/nrn2667

60. Borghesani V, Pedregosa F, Buiatti M, Amadon A, Eger E, Piazza M. Word meaning in the ventral visual path: a perceptual to conceptual gradient of semantic coding. Neuroimage. 2016;143: 128–140. doi:10.1016/j.neuroimage.2016.08.068

61. Goodale MA, Milner AD. Separate Visual Pathways for Perception and Action. Trends Neurosci. 1992;15: 20–25. doi:10.1016/0166-2236(92)90344-8

62. Braga RM, Hellyer PJ, Wise RJS, Leech R. Auditory and visual connectivity gradients in frontoparietal cortex. Hum Brain Mapp. 2017;38: 255–270. doi:10.1002/hbm.23358

63. Passingham RE, Stephan KE, Kötter R. The anatomical basis of functional localization in the cortex. Nat Rev Neurosci. 2002;3: 606–616. doi:10.1038/nrn893

64. Crone EA, Elzinga BM. Changing brains: how longitudinal functional magnetic resonance imaging studies can inform us about cognitive and social-affective growth trajectories. Wiley Interdiscip Rev Cogn Sci. 2015;6: 53–63. doi:10.1002/wcs.1327

65. McCormick EM, Qu Y, Telzer EH. Activation in context: Differential conclusions drawn from cross-sectional and longitudinal analyses of adolescents' cognitive control-related neural activity. Front Hum Neurosci. 2017;11: 141. doi:10.3389/fnhum.2017.00141

66. McCormick EM, Telzer EH. Adaptive Adolescent Flexibility: Neurodevelopment of Decision-making and Learning in a Risky Context. J Cogn Neurosci. 2017;29: 413–423. doi:10.1162/jocn_a_01061

67. Supekar K, Uddin LQ, Prater K, Amin H, Greicius MD, Menon V. Development of functional and structural connectivity within the default mode network in young children. Neuroimage. 2010;52: 290–301. doi:10.1016/j.neuroimage.2010.04.009

68. Uddin LQ, Supekar KS, Ryali S, Menon V. Dynamic reconfiguration of structural and functional connectivity across core neurocognitive brain networks with development. J Neurosci. 2011;31: 18578–18589. doi:10.1523/JNEUROSCI.4465-11.2011

69. Ziegler G, Hauser TU, Moutoussis M, Bullmore ET, Goodyer IM, Fonagy P, et al. Compulsivity and impulsivity traits linked to attenuated developmental frontostriatal myelination trajectories. Nat Neurosci. 2019;22: 992–999. doi:10.1038/s41593-019-0394-3

70. Genc S, Malpas CB, Gulenc A, Sciberras E, Efron D, Silk TJ, et al. Longitudinal patterns of white matter fibre density and morphology in children are associated with age and pubertal stage. Dev Cogn Neurosci. 2020;45: 100853. doi:10.1016/j.dcn.2020.100853

71. Oldham S, Fornito A. The development of brain network hubs. Dev Cogn Neurosci. 2019;36: 100607. doi:10.1016/j.dcn.2018.12.005

72. Dennis EL, Jahanshad N, McMahon KL, de Zubicaray GI, Martin NG, Hickie IB, et al. Development of brain structural connectivity between ages 12 and 30: A 4-Tesla diffusion imaging study in 439 adolescents and adults. Neuroimage. 2013;64: 671–684. doi:10.1016/j.neuroimage.2012.09.004

73. Khundrakpam BS, Lewis JD, Zhao L, Chouinard-Decorte F, Evans AC. Brain connectivity in normally developing children and adolescents. Neuroimage. 2016;134: 192–203. doi:10.1016/j.neuroimage.2016.03.062

74. Sowell ER, Peterson BS, Thompson PM, Welcome SE, Henkenius AL, Toga AW. Mapping cortical change across the human life span. Nat Neurosci. 2003;6: 309–315. doi:10.1038/nn1008

75. Steinbeis N, Bernhardt BC, Singer T. Impulse Control and Underlying Functions of the Left DLPFC Mediate Age-Related and Age-Independent Individual Differences in Strategic Social Behavior. Neuron. 2012;73: 1040–1051. doi:10.1016/j.neuron.2011.12.027

76. Weiskopf N, Suckling J, Williams G, Correia M. MM, Inkster B, Tait R, et al. Quantitative multi-parameter mapping of R1, PD*, MT, and R2* at 3T: A multi-center validation. Front Neurosci. 2013;7: 95. doi:10.3389/fnins.2013.00095

77. Avants BB, Tustison NJ, Song G, Cook PA, Klein A, Gee JC. A reproducible evaluation of ANTs similarity metric performance in brain image registration. Neuroimage. 2011;54: 2033–2044. doi:10.1016/j.neuroimage.2010.09.025

78. Cox RW. AFNI : Software for Analysis and Visualization of Functional Magnetic Resonance Neuroimages. Comput Biomed Res. 1996;29: 162–173. doi:10.1006/cbmr.1996.0014

79. Fischl B. FreeSurfer. Neuroimage. 2012;62: 774–781. doi:10.1016/j.neuroimage.2012.01.021

80. Jenkinson M, Beckmann CF, Behrens TEJ, Woolrich MW, Smith SM. Fsl. Neuroimage. 2012;62: 782–790. doi:10.1016/j.neuroimage.2011.09.015

81. Park B, Byeon K, Park H. FuNP (Fusion of Neuroimaging Preprocessing) Pipelines: A Fully Automated Preprocessing Software for Functional Magnetic Resonance Imaging. Front Neuroinform. 2019;13: 5. doi:10.3389/fninf.2019.00005

82. Glasser MF, Sotiropoulos SN, Wilson JA, Coalson TS, Fischl B, Andersson JL, et al. The minimal preprocessing pipelines for the Human Connectome Project. Neuroimage. 2013;80: 105–124. doi:10.1016/j.neuroimage.2013.04.127

83. Dale AM, Fischl B, Sereno MI. Cortical surface-based analysis: I. Segmentation and surface reconstruction. Neuroimage. 1999;9: 179–194. doi:10.1006/nimg.1998.0395

84. Fischl B, Sereno MI, Dale AM. Cortical surface-based analysis: II. Inflation, flattening, and a surface-based coordinate system. Neuroimage. 1999;9: 195–207. doi:10.1006/nimg.1998.0396

85. Fischl B, Sereno MI, Tootell RBH, Dale AM. High-resolution inter-subject averaging and a surface-based coordinate system. Hum Brain Mapp. 1999;8: 272–284. doi:10.1002/(SICI)1097-0193(1999)8

86. Kundu P, Brenowitz ND, Voon V, Worbe Y, Vértes PE, Inati SJ, et al. Integrated strategy for improving functional connectivity mapping using multiecho fMRI. Proc Natl Acad Sci U S A. 2013;110: 16187–16192. doi:10.1073/pnas.1301725110

87. Kundu P, Inati SJ, Evans JW, Luh WM, Bandettini PA. Differentiating BOLD and non-BOLD signals in fMRI time series using multi-echo EPI. Neuroimage. 2012;60: 1759–1770. doi:10.1016/j.neuroimage.2011.12.028

88. Legland D, Beaugrand J. Automated clustering of lignocellulosic fibres based on morphometric features and using clustering of variables. Ind Crops Prod. 2013;45: 253–261. doi:10.1016/j.indcrop.2012.12.021

89. Smith RE, Tournier JD, Calamante F, Connelly A. Anatomically-constrained tractography: Improved diffusion MRI streamlines tractography through effective use of anatomical information. Neuroimage. 2012;62: 1924–1938. doi:10.1016/j.neuroimage.2012.06.005

90. Christiaens D, Reisert M, Dhollander T, Sunaert S, Suetens P, Maes F. Global tractography of multi-shell diffusion-weighted imaging data using a multi-tissue model. Neuroimage.

2015;123: 89–101. doi:10.1016/j.neuroimage.2015.08.008

91. Jeurissen B, Tournier JD, Dhollander T, Connelly A, Sijbers J. Multi-tissue constrained spherical deconvolution for improved analysis of multi-shell diffusion MRI data. Neuroimage. 2014;103: 411–426. doi:10.1016/j.neuroimage.2014.07.061

92. Tournier J-D, Calamante F, Connelly A. Improved probabilistic streamlines tractography by 2 nd order integration over fibre orientation distributions. Proceedings of the International Society for Magnetic Resonance in Medicine. 2010. p. 1670.

93. Smith RE, Tournier JD, Calamante F, Connelly A. SIFT2: Enabling dense quantitative assessment of brain white matter connectivity using streamlines tractography. Neuroimage. 2015;119: 338–351. doi:10.1016/j.neuroimage.2015.06.092

94. Amico E, Goñi J. Mapping hybrid functional-structural connectivity traits in the human connectome. Netw Neurosci. 2018;2: 306–322. doi:10.1162/netn_a_00049

95. Fornito A, Zalesky A, Bullmore E. Fundamentals of Brain Network Analysis. Amsterdam: Academic Press; 2016.

96. Tenenbaum JB, Silva V de, Langford JC. A Global Geometric Framework for Nonlinear Dimensionality Reduction. Science (80-). 2000;290: 2319–2323. doi:10.1126/science.290.5500.2319

97. von Luxburg U. A tutorial on spectral clustering. Stat Comput. 2007;17: 395–416. doi:10.1007/s11222-007-9033-z

98. Hong S-J, Vos De Wael R, Bethlehem RAI, Lariviere S, Paquola C, Valk SL, et al. Atypical functional connectome hierarchy in autism. Nat Commun. 2019;10: 1022.

99. Park B, Hong S, Valk SL, Paquola C, Benkarim O, Bethlehem RAI, et al. Differences in subcortico-cortical interactions identified from connectome and microcircuit models in autism. Nat Commun. 2021;12: 2225. doi:10.1038/s41467-021-21732-0

100. Langs G, Golland P, Ghosh SS. Predicting Activation Across Individuals with Resting-State Functional Connectivity Based Multi-Atlas Label Fusion. International Conference on Medical Image Computing and Computer-Assisted Intervention. 2015. pp. 313–320. doi:10.1007/978-3-319-24571-3_38

101. Bethlehem RAI, Paquola C, Seidlitz J, Ronan L, Bernhardt B, Consortium CCAN, et al. Dispersion of functional gradients across the adult lifespan. Neuroimage. 2020;222: 117299. doi:10.1016/j.neuroimage.2020.117299

102. Benjamini Y, Hochberg Y. Controlling the False Discovery Rate : A Practical and Powerful Approach to Multiple Testing. J R Stat Soc. 1995;57: 289–300.

103. Alexander-Bloch AF, Shou H, Liu S, Satterthwaite TD, Glahn DC, Shinohara RT, et al. On testing for spatial correspondence between maps of human brain structure and function. Neuroimage. 2018;178: 540–551. doi:10.1016/j.neuroimage.2018.05.070

Supporting Information

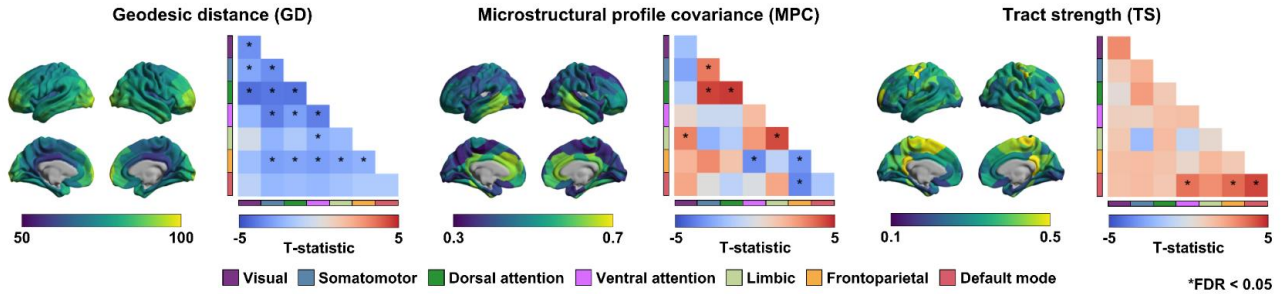

Fig. S1 | Age-effects on each cortical wiring feature. The spatial maps of GD, MPC, and TS are shown on the brain surface. The t-statistics of age-related changes on each cortical feature within- and between-networks, with significant (FDR < 0.05) results marked with asterisks. *Abbreviation:* FDR, false discovery rate.

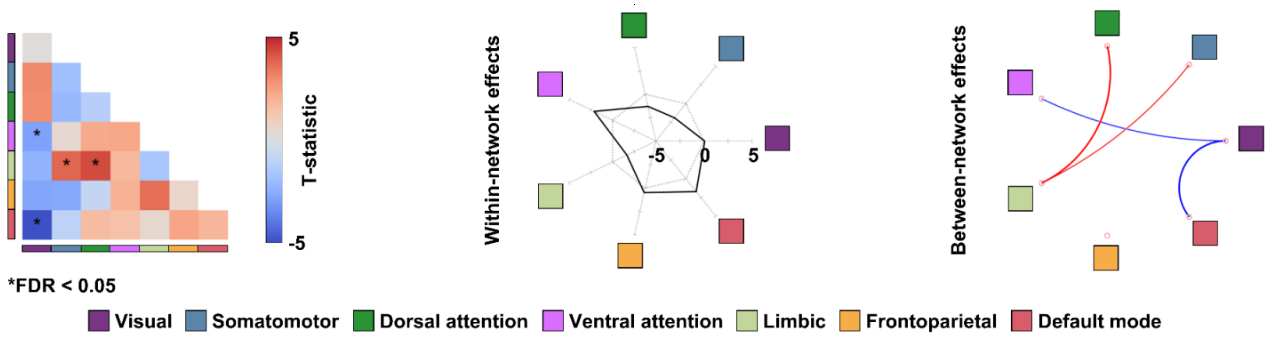

Fig. S2 | Age-effects on multiscale cortical wiring distance after controlling for mean wiring distance. The t-statistics of age-effects are reported in the matrix, and within- and between-network effects are represented with radar and circular plots, respectively. For details, see *Fig. 1*.

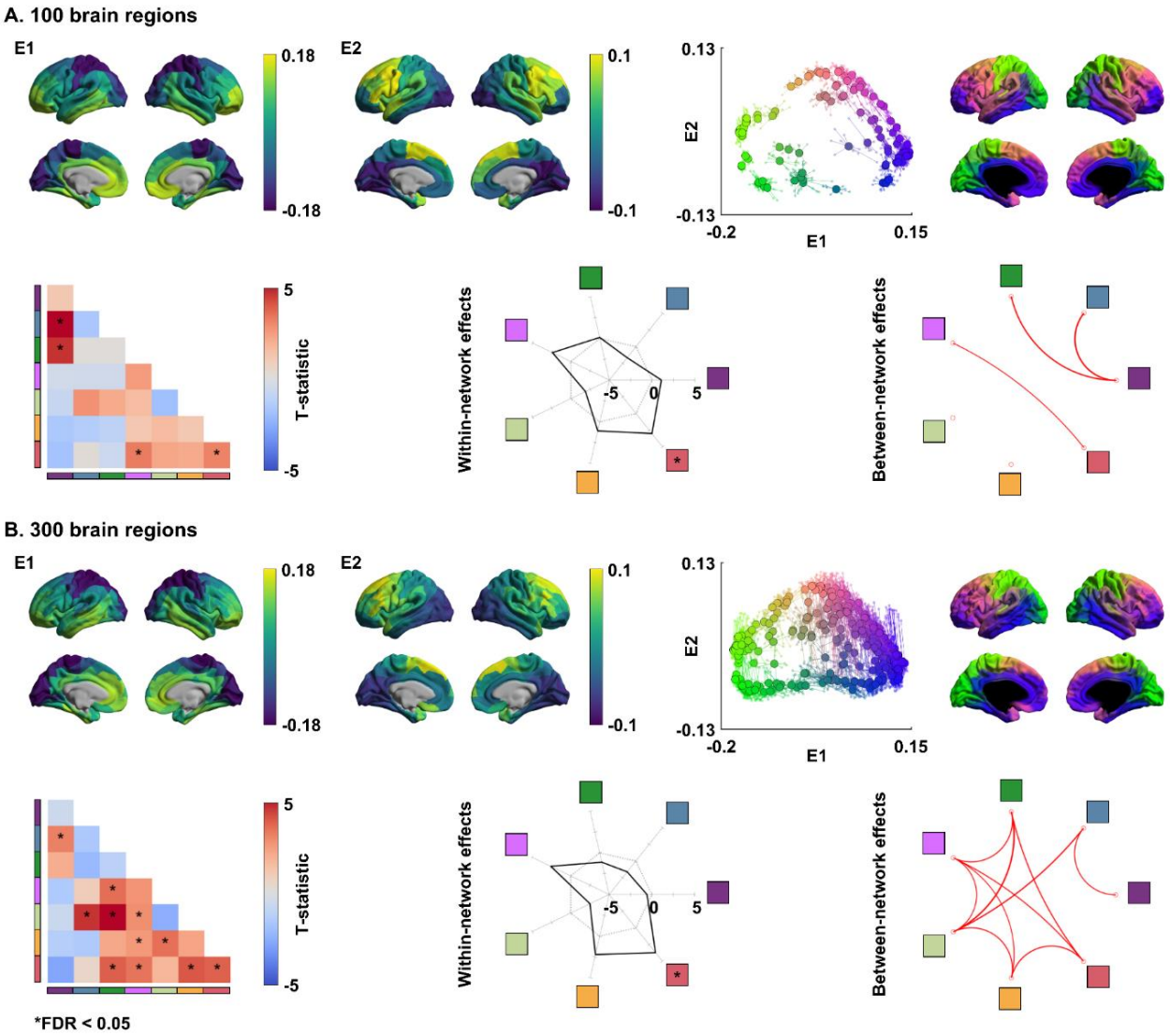

Fig. S3 | Structural manifolds and age-effects on multiscale cortical wiring distance using different parcellation scales. (A) Results using 100 and **(B)** 300 parcellations. Two eigenvectors (E1, E2) estimated from the cortical wiring features (top) and t-statistics of age-effects within- and between-networks (bottom) are reported. For details, see *Fig. 1*.

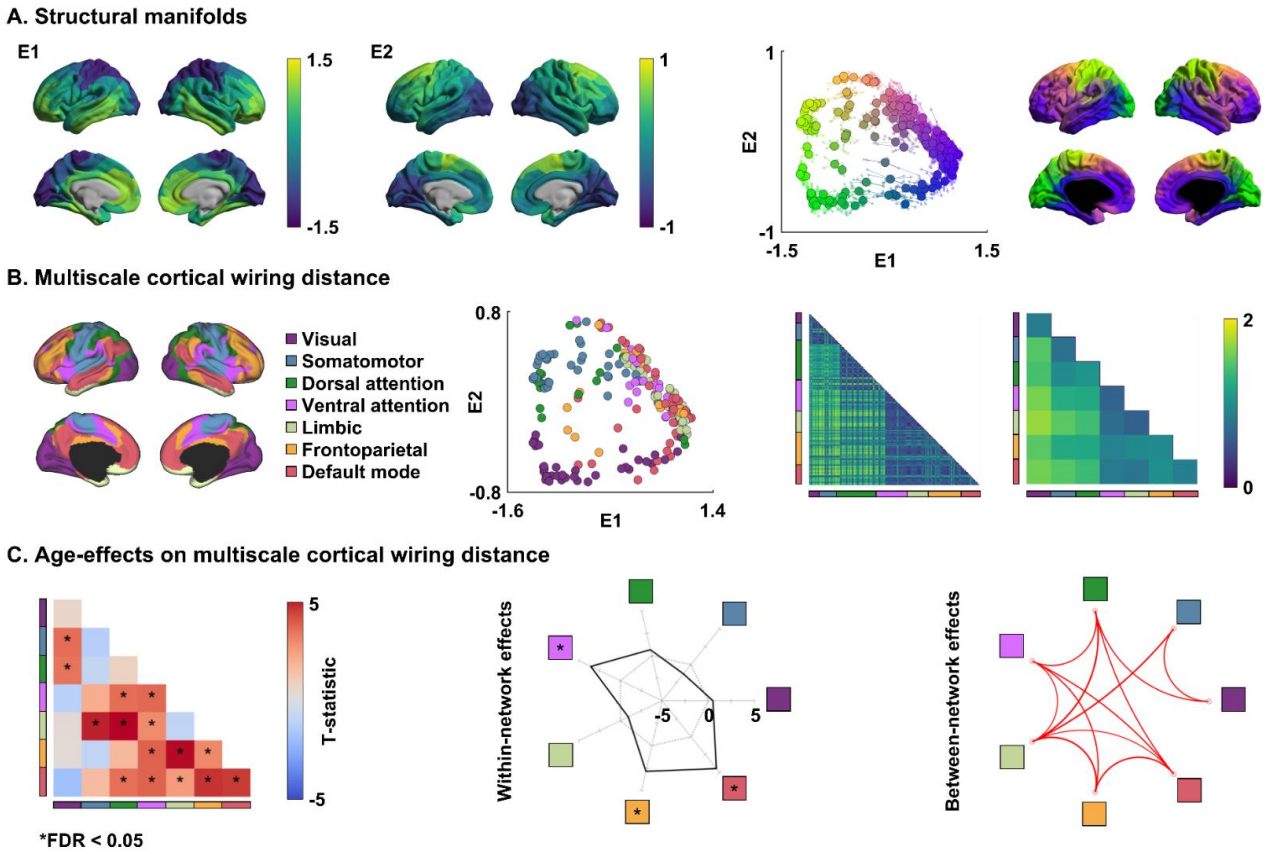

Fig. S4 | Structural manifolds derived using principal component analysis and age-effects on multiscale cortical wiring distance. (A) Two eigenvectors (E1, E2) estimated from the cortical wiring features. **(B)** The wiring distance summarized based on functional communities. **(C)** The t-statistics of age-effects on wiring distance within- and between-networks. For details, see *Fig. 1*.

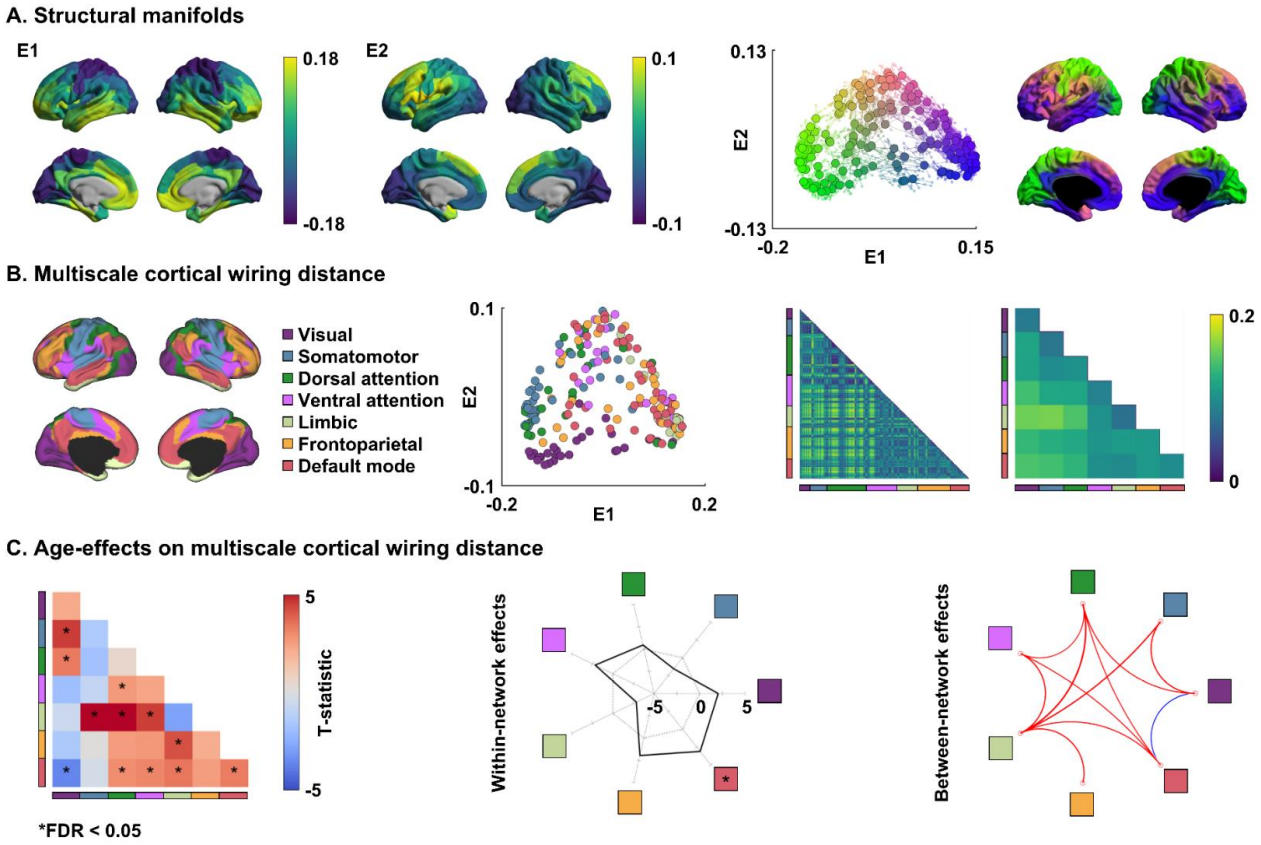

Fig. S5 | Structural manifolds and age-effects on multiscale cortical wiring distance using Schaefer 200 parcellation. (A) Two eigenvectors (E1, E2) estimated from the cortical wiring features. **(B)** The wiring distance summarized based on functional communities. **(C)** The t-statistics of age-effects on wiring distance within- and between-networks. For details, see *Fig. 1*.

Neuroscience in Psychiatry Network (NSPN) Consortium author list

Principal investigators:

Edward Bullmore (CI from 01/01/2017)[1,2,3]; Raymond Dolan[4,5]; Ian Goodyer (CI until 01/01/2017)[1]; Peter Fonagy[6]; Peter Jones[1]

NSPN (funded) staff:

Michael Moutoussis[4,5]; Tobias Hauser[4,5]; Sharon Neufeld[1]; Rafael Romero-Garcia[1,2]; Michelle St Clair[1]; Petra Vértes[1,2]; Kirstie Whitaker[1,2]; Becky Inkster[1]; Gita Prabhu[4,5]; Cinly Ooi[1]; Umar Toseeb[1]; Barry Widmer[1]; Junaid Bhatti[1]; Laura Villis[1]; Ayesha Alrumaithi[1]; Sarah Birt[1]; Aislinn Bowler[5]; Kalia Cleridou[5]; Hina Dadabhoy[5]; Emma Davies[1]; Ashlyn Firkins[1]; Sian Granville[5]; Elizabeth Harding[5]; Alexandra Hopkins[4,5]; Daniel Isaacs[5]; Janchai King[5]; Danae Kokorikou[5,6]; Christina Maurice[1]; Cleo McIntosh[1]; Jessica Memarzia[1]; Harriet Mills[5]; Ciara O'Donnell[1]; Sara Pantaleone[5]; Jenny Scott[1]; Beatrice Kiddle[1]; Ela Polek[1]

Affiliated scientists:

Pasco Fearon[6]; John Suckling[1]; Anne-Laura van Harmelen[1]; Rogier Kievit[4,7]; Sam Chamberlain[1]

[1]Department of Psychiatry, University of Cambridge, United Kingdom
[2]Behavioural and Clinical Neuroscience Institute, University of Cambridge, United Kingdom
[3]ImmunoPsychiatry, GlaxoSmithKline Research and Development, United Kingdom
[4]Max Planck University College London Centre for Computational Psychiatry and Ageing Research, University College London, UK
[5]Wellcome Centre for Human Neuroimaging, University College London, United Kingdom
[6]Research Department of Clinical, Educational and Health Psychology, University College London, United Kingdom
[7]Medical Research Council Cognition and Brain Sciences Unit, University of Cambridge, United Kingdom